Iron Speciation of Airborne Subway Particles by the Combined Use of Energy Dispersive Electron Probe X-ray Microanalysis and Raman Microspectrometry

ARTICLE *in* ANALYTICAL CHEMISTRY · SEPTEMBER 2013

Impact Factor: 5.64 · DOI: 10.1021/ac402406n · Source: PubMed

8 AUTHORS, INCLUDING:

Youn-Suk Son
Korea Atomic Energy Research Institute (KAERI)
39 PUBLICATIONS **169** CITATIONS
SEE PROFILE

Jo-Chun Kim
Konkuk University
79 PUBLICATIONS **747** CITATIONS
SEE PROFILE

Young Sunwoo
Konkuk University
39 PUBLICATIONS **665** CITATIONS
SEE PROFILE

Chul-Un Ro
Inha University
100 PUBLICATIONS **1,580** CITATIONS
SEE PROFILE

analytical chemistry

Article

pubs.acs.org/ac

Iron Speciation of Airborne Subway Particles by the Combined Use of Energy Dispersive Electron Probe X-ray Microanalysis and Raman Microspectrometry

Hyo-Jin Eom,[†] Hae-Jin Jung,[†] Sophie Sobanska,[‡] Sang-Gwi Chung,[§] Youn-Suk Son,[§,⊥] Jo-Chun Kim,[§,∥] Young Sunwoo,[§] and Chul-Un Ro*[,†]

[†]Department of Chemistry, Inha University, 253, Yonghyun-dong, Nam-gu, Incheon 402-751, Korea

[‡]Laboratoire de Spectrochimie Infrarouge et Raman, UMR CNRS 8516, Université de Lille 1, Bât. C5, 59655 Villeneuve d'Ascq, Cedex, France

[§]Department of Advanced Technology Fusion, Konkuk University, Seoul 143-701, Korea

[∥]Department of Environmental Engineering, Konkuk University, Seoul 143-701, Korea

Supporting Information

ABSTRACT: Quantitative energy-dispersive electron probe X-ray microanalysis (ED-EPMA), known as low-*Z* particle EPMA, and Raman microspectrometry (RMS) were applied in combination for an analysis of the iron species in airborne PM_{10} particles collected in underground subway tunnels. Iron species have been reported to be a major chemical species in underground subway particles generated mainly from mechanical wear and friction processes. In particular, iron-containing particles in subway tunnels are expected to be generated with minimal outdoor influence on the particle composition. Because iron-containing particles have different toxicity and magnetic properties depending on their oxidation states, it is important to determine the iron species of underground subway particles in the context of both indoor public health and control measures. A recently developed analytical methodology, i.e., the combined use of low-*Z* particle EPMA and RMS, was used to identify the chemical species of the same individual subway particles on a single particle basis, and the bulk iron compositions of airborne subway particles were also analyzed by X-ray diffraction. The majority of airborne subway particles collected in the underground tunnels were found to be magnetite, hematite, and iron metal. All the particles collected in the tunnels of underground subway stations were attracted to permanent magnets due mainly to the almost ubiquitous ferrimagnetic magnetite, indicating that airborne subway particles can be removed using magnets as a control measure.

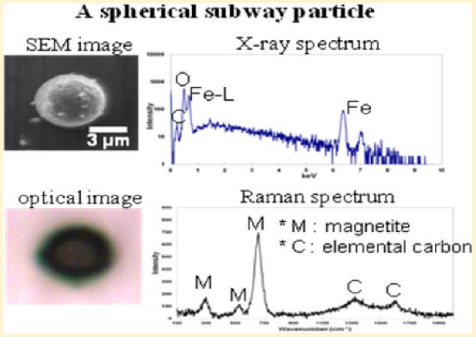

People spend most of their time indoors, either at home, in the workplace, or in transit, and there has been increasing concern over the air quality of indoor microenvironments and its effects on public health. Among the various types of indoor microenvironments, underground subway stations have unique characteristics in that they are relatively closed spaces with strong indoor particle emission sources. Airborne subway particles, which are generated mainly by the movement of trains and passengers, can accumulate in this rather closed environment, resulting in high concentrations of indoor particulate matter (PM), which has been reported in many subway systems worldwide.[1−10] As many people within metropolitan areas worldwide commute using underground subway transportation and spend considerable time in the underground subway environment on a daily basis, there has been increasing concern regarding the air quality in underground subway systems because of the possible adverse effects on public health.[5,11−19]

The major chemical species of underground subway particles have been reported to be iron-containing particles that are generated mainly from mechanical wear and friction processes at rail-wheel-brake interfaces and at the interface between the catenaries providing electricity to subway trains and pantographs attached to the trains.[4,5,11,18,20] The subway particle samples collected by commuters using the London Underground system contained the most Fe/Si-rich particles comprising 53% of the total number of particles.[20] For $PM_{2.5}$ subway samples collected at London Underground stations (where PM_x indicates particulate matters of aerodynamic diameter smaller than x μm), iron oxide particles were the majority (67% in weight fraction).[5] Subway samples collected in New York, Helsinki, Tokyo, and Budapest also contained very high concentrations of iron (42% of $PM_{2.5}$, 88−92% of $PM_{2.5}$, 74% of SPM, 40−46% of PM_{10}, respectively, where SPM is the abbreviation of suspended PM).[4,11,18] For eight samples collected twice in each season at the platform of an

Received: July 31, 2013
Accepted: September 27, 2013
Published: September 27, 2013

underground subway station in Seoul, Korea, iron-containing particles were encountered most frequently, with relative abundances in the range of 61−79%.[21] Most the iron-containing particles were observed to exist as oxidized forms.

Iron-containing subway particles can be in the form of iron metal (α-Fe), hematite (α-Fe_2O_3), maghemite (γ-Fe_2O_3), and/or magnetite (Fe_3O_4) that have different toxicity and magnetic properties. A comparison of the genotoxicity of different particle types collected from wood and pellet combustion, tire-road wear, an urban street, and subway stations revealed the particles from the subway stations to be the most genotoxic.[13] Other studies also reported that underground subway particles have cytotoxic and inflammatory potential as well as transient biological effects,[5,14,15] and the toxicity of subway particles was attributed to the high iron content.[22] Subway particles collected in a subway station in Stockholm, Sweden, were found to be 8 times more genotoxic than urban street particles because iron-containing subway particles were found to be in the form of magnetite, which has adverse health effects.[12] On the other hand, major iron oxide particles collected at a subway station in Budapest, Hungary, were reported to be mainly relatively harmless hematite with only small amounts of magnetite.[18] A recent X-ray diffraction (XRD) study revealed hematite to be the major particle type in particles collected at a subway station in Barcelona, Spain.[23] Although studies of the iron species in airborne subway particles are limited, the reported differences in the iron particle types can be attributed to different subway systems such as rail, wheel, braking mechanism, ventilation, air conditioning, etc.[3,23]

At room temperature, hematite is a canted antiferromagnet, whereas iron metal is ferromagnetic and maghemite and magnetite are ferrimagnetic. If iron-containing subway particles are strongly magnetic such as iron metal, maghemite, and magnetite, the subway PM levels could be reduced effectively using magnets. Recently, XRD analysis of floor dust collected at subway platforms in Shanghai, China revealed iron metal and magnetite with small amounts of hematite. The particles showed extremely strong magnetic signatures.[24] In a recent study,[25] all floor dusts of <25 μm size fractions collected in an underground subway station in Seoul, Korea, were attracted to permanent magnets and iron metal, which is relatively harmless, was the main chemical species in the floor dust.

In other studies,[26,27] iron-containing particles, mostly in the form of iron oxides, were also found to be the most abundant in airborne samples collected at different locations (in tunnels, at platforms, and near ticket offices) of underground subway stations in Seoul, Korea. For the samples collected in tunnels, iron-containing particles predominate with relative abundances of 75−91%. The amounts of iron-containing particles decreased with increasing distance of the sampling locations from the tunnel, which strongly suggests that the iron-containing particles originated in tunnels.

As iron-containing particles predominating in underground subway systems are generated in tunnels, where the outdoor influence on the chemical compositions of the iron-containing subway particles is minimal, the airborne subway particles collected in tunnels could be useful for the study of iron species generated in subway microenvironments. Recently, an analytical methodology that combines a quantitative energy-dispersive electron probe X-ray microanalysis (ED-EPMA), known as low-Z particle EPMA, and Raman microspectrometry (RMS) techniques for the analysis of the same individual particles of micrometer size was reported.[28] In that study, low-Z particle EPMA and RMS were applied in combination for the first time to characterize the complex internal structure and physicochemical properties of the same ensemble of Asian dust particles. In addition, individual particles, including chemical speciation and mixing state analysis, can be characterized better in detail using low-Z particle EPMA and RMS in combination than with the two single-particle techniques alone. In this study, the recently developed analytical methodology was used to clearly elucidate iron species of the same individual subway particles in airborne PM_{10} samples collected in the tunnels of two underground subway stations in Seoul, Korea, on a single particle basis.

EXPERIMENTAL SECTION

Samples. Seoul, the capital of Korea, is a densely populated megacity (population 10.5 million, area 605 km^2). The Seoul subway system contains 9 lines with a total of 412 stations. According to the statistics from the Seoul metro transportation center (http://www.seoulmetro.co.kr), approximately 6.8 million commuters use the Seoul subway system on a daily basis. For the rails, wheels, and pantographs, the high carbon steel containing minor amounts of C (0.6−0.75%), Si (0.1−0.3%), Mn (0.7−1.1%), P (<0.035%), and S (0.04%) is used. In this study, airborne subway samples were collected using PM_{10} cyclone samplers (URG-2000-30ENB, URG), from the tunnels of two underground subway stations in Seoul, namely, "Daechung" and "Yangjae" stations, which are among the busiest subway stations in Seoul, with 12 000 and 44 000 commuters per day, respectively. The platforms and rails of the two stations are two stories below the urban street level. The samplers were located in the tunnels ∼100 m away from the platforms. As bulk XRD analysis requires a significant particle sample mass, four PM_{10} cyclone samplers were used together for sampling in each tunnel. Each sampling period lasted for 40 h, and sampling was repeated three times for 7 days in each station (see Table S1 in Supporting Information for the sampling dates, durations, total sample mass, etc.). During the sampling periods, temperature and humidity in the sampling places were almost constant (i.e., temperature = 12−15 °C and relative humidity = 40−50%).

The particles were collected on Nuclepore polycarbonate (PC) filters (pore size 0.4 μm), and all filters with particles obtained at each station were dissolved in chloroform. As iron-containing subway particles are heavier than chloroform, the particles sank to the bottom of the beaker over a 2 day period and the upper part of the solution was removed using a pipet. The procedure was repeated three times to ensure complete separation of the particles from the PC filters. The absence of polycarbonate species in the solution was confirmed by the absence of its characteristic IR peaks in the attenuated total reflectance FTIR spectra. The particle samples obtained after drying the solutions are denoted as samples S1 and S2 for those collected in tunnels of Daechung and Yangjae stations, respectively.

For the single particle analysis by low-Z particle EPMA and RMS, the particles were transferred on either Ag or Al foils. The foils were simply rubbed over the surface of the particle samples and particles adhered on the foils. In this study, ∼160 particles for each sample were analyzed both by low-Z particle EPMA and RMS.

Low-Z Particle EPMA Measurement. Low-Z particle EPMA, a quantitative single particle analysis, was used to collect morphological and elemental compositional information on the

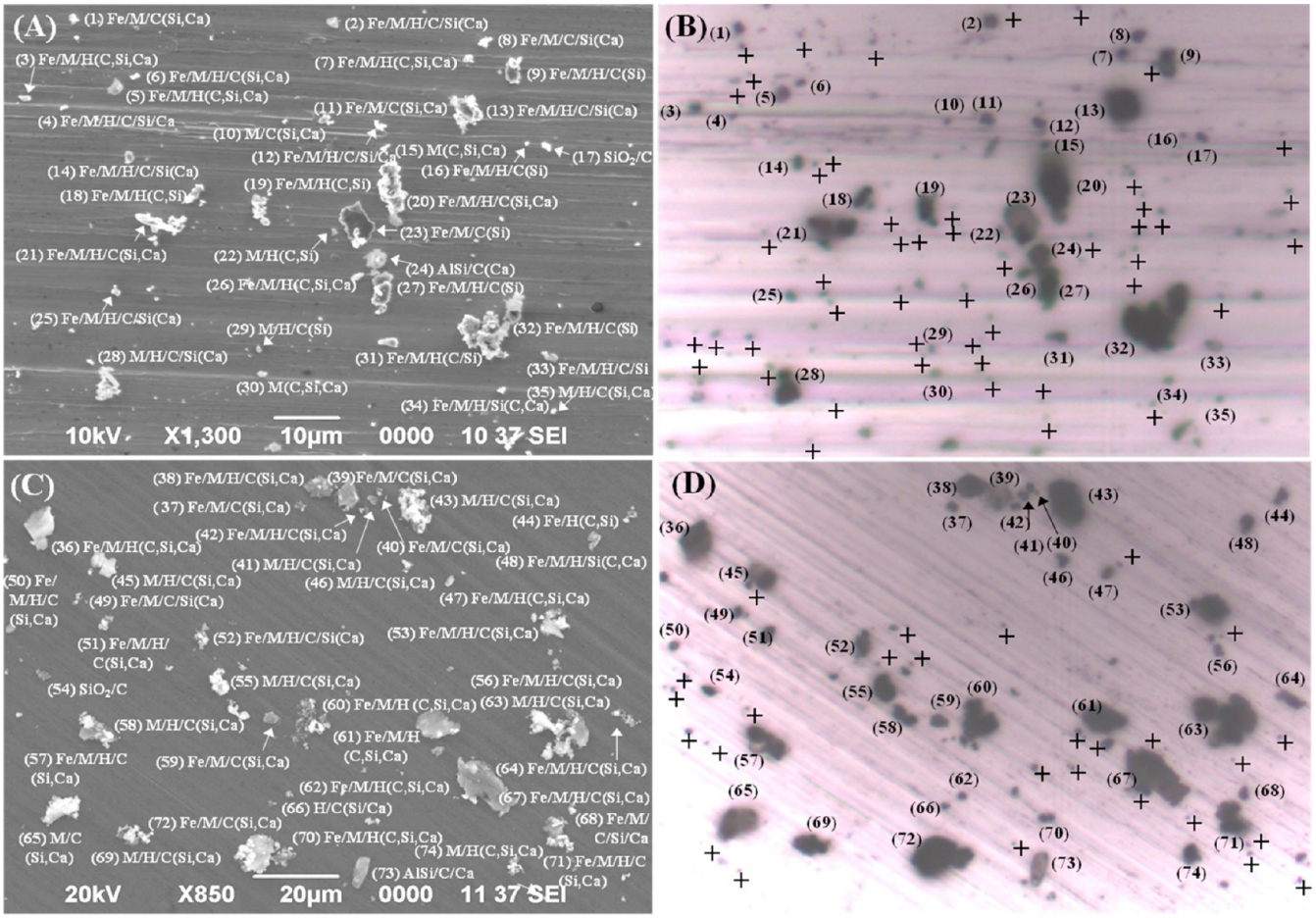

Figure 1. Secondary electron and visible optical images of the same image fields for sample S1 ((parts A and B, respectively) and sample S2 (parts C and D, respectively).

individual particles. The measurements were carried out on a scanning electron microscope (JEOL JSM-6390) equipped with an Oxford Link SATW ultrathin window Si(Li) EDX detector with a resolution of 133 eV for the Mn−Kα X-rays. The X-ray spectra were recorded under the control of EMAX Oxford software. A 10 kV accelerating voltage was used to achieve the optimal experimental conditions, such as a low background level in the spectra and high sensitivity for low-Z element analysis. The beam current was 0.5 nA, and a typical measuring time of 15 s was used to obtain a sufficient count in the EDX spectra. A more detailed discussion of the measurement conditions is reported elsewhere.[29] EDX data acquisition for the individual particles was carried out manually in point analysis mode, whereby the electron beam was focused on the center of each particle and the X-rays were acquired while the beam remained fixed on this single spot.

The net X-ray intensities of the elements were obtained by a nonlinear least-squares fitting of the spectra collected using the AXIL program.[30] The elemental concentrations of the individual particles were determined from their X-ray intensities using a Monte Carlo calculation combined with reverse successive approximations.[31−33] The quantification procedure provided accurate results within 12% relative deviations between the calculated and nominal elemental concentrations when the method was applied to various standard particles, such as NaCl, Al_2O_3, $CaSO_4{\cdot}2H_2O$, Fe_2O_3, $CaCO_3$, and KNO_3.[31,33,34]

RMS Measurement. The foils with particles were placed on the microscope stage of a confocal Raman microspectrometer (LabRAM, Horiba Jobin-Yvon) equipped with a 100×, 0.9 numerical aperture objective (Olympus). Raman scattering was performed at a wavelength of 632.8 nm using a He−Ne laser and detected with a N_2-cooled charge-coupled device (CCD) detector. The laser power delivered to the sample was approximately 0.7 mW and could be attenuated by a set of neutral density filters with an optical density ranging from 0.3 to 4. The spot size of the laser at the sample was estimated to be ∼1 μm^2. A confocal hole, 500 μm in diameter, was used, giving an axial resolution (Z) of approximately 3.4 μm. The spectra were acquired using Labspec software. For each analysis, the spectral range of 140−2000 cm^{-1} was explored with a 30 s acquisition time in ambient relative humidity (RH = ∼60%). The absence of laser damage to the sample was confirmed by comparing the optical images recorded before and after Raman mapping.

Combined Use of Low-Z Particle EPMA and RMS for the Iron Speciation of Iron-Containing Individual Subway Particles. Single particle analysis based on low-Z particle EPMA can distinguish the iron metal particles clearly from iron oxides because the morphology and Fe and O contents of the iron metal and oxides are different. On the other hand, the quantitative elemental concentration data obtained by low-Z particle EPMA were not sufficiently useful to differentiate the iron oxides, such as hematite, maghemite, and magnetite

dx.doi.org/10.1021/ac402406n | Anal. Chem. 2013, 85, 10424−10431

because the inaccuracy involved in the quantification can be ~12% and, more importantly, iron oxide particles can exist in partially oxidized forms.[21] RMS can clearly differentiate hematite, maghemite, and magnetite and can also detect the presence of each iron oxide species even when two oxides are mixed internally in the individual particles. On the other hand, RMS cannot detect iron metal because it is Raman inactive. In this study, ~160 particles for each sample were analyzed, totaling 320 particles for samples S1 and S2, where the same individual particles were analyzed by both low-*Z* particle EPMA and RMS. First, low-*Z* particle EPMA measurements were performed to obtain the morphological and X-ray spectral data of the individual particles, followed by RMS measurements to obtain the Raman spectral data of the same individual particles examined previously by low-*Z* particle EPMA after the particles were relocated using secondary electron and optical images, which were recorded with a similar magnification and manner to that described previously.[35] The combined application of two single particle analytical techniques, such as low-*Z* particle EPMA and RMS, for the characterization of the same individual particles is a new analytical methodology. The first application of this methodology was described in a recent paper, where details of the methodology can be found.[28] Morphological, X-ray spectral, and Raman spectral data of each particle obtained by the combined use of low-*Z* particle EPMA and RMS were used to clearly identify the iron species in the particle.

XRD Measurement for Bulk Analysis. To determine the bulk chemical species of airborne subway particles, XRD (Rigaku DMAX-2500) was performed using Cu Kα radiation. The 2θ scanning range, scanning speed, and step size were 10–90°, 3°/min, and 0.02° 2θ, respectively. The structures were identified using the standard powders and JCPDS card database. The standard powders included iron metal (Sigma-Aldrich, 99%), hematite (α-Fe_2O_3, Sigma-Aldrich, ≥99%), maghemite (γ-Fe_2O_3, Kojundo, 99%), magnetite (Fe_3O_4, Sigma-Aldrich, 98%), $CaCO_3$ (Sigma-Aldrich, ≥99.995%), and SiO_2 (Sigma-Aldrich, ≥99.995%).

RESULTS AND DISCUSSION

Combined Use of Low-*Z* Particle EPMA and RMS for Iron Speciation of Individual Particles. Two single particle analytical techniques such as low-*Z* particle EPMA and RMS were applied in combination to analyze the same individual particles for samples S1 and S2. First, 154 and 166 individual particles for samples S1 and S2, respectively, were examined using low-*Z* particle EPMA to obtain information on their morphology and elemental compositions on a single particle basis. Metal foil samples, ~1 × 1 cm^2 size, were transferred off-line to the Raman instrument, where the optical microscope installed in the Raman instrument was used to relocate the same image fields examined by low-*Z* particle EPMA. Figure 1 shows secondary electron images (SEIs) from SEM and the visible optical images from the Raman microspectrometer of the same exemplar image fields for samples S1 and S2. Although the image quality of the SEIs and optical images were different due to the different spatial resolutions available in SEM and optical microscopy, the optical image quality was sufficient for the relocation of the same image fields examined by low-*Z* particle EPMA. The same patterns of particle location among the SEI and optical image, where the same particles were notated as the same particle numbers, ensured that the same micrometer-sized particles were analyzed.

As shown in the SEIs, a unique notation was devised to describe the chemical species of the individual particles, e.g., the notation "Fe/M/C(Si,Ca)" for particle no. 11 in Figure 1A indicates that the particle is iron metal and magnetite mixed internally with C at >5 at % and Si and Ca (put in the parentheses) at <5 at %, where the chemical species were identified by the combined interpretation of two spectral data sets of low-*Z* particle EPMA and RMS obtained for the same individual particles. In order not to make the particle notations too crowded on the SEIs, magnetite and hematite were notated as "M" and "H", respectively. As shown in Figure 1A,C, most of the particles were iron metal and iron oxides mixed with other elements, such as C, Si, and/or Ca. No significant differences were observed between samples S1 and S2, indicating that the generation mechanism of subway particles in tunnels is the same.

Iron metal particles appear dark and sliced (flat) in shape on their SEIs, such as particle no. 23 in Figure 1A, whereas the iron oxides appear bright and angular like many other particles in Figure 1A,C. The different brightness between the iron metal and oxides results mainly from the different secondary electron yields between the conducting metal and insulating oxide particles, where the insulating oxide particles develop a negative charge due to the accumulation of primary electrons, resulting in brighter contrast from the larger emission of secondary electrons by repulsion, in addition to the edge and inclined angle effects.[36] The iron metal particles of comparatively large size present the sliced forms because they were generated from scraps broken off from the train wheels or rails. In addition to their different SEI of iron metal particles, the X-ray spectral data can help distinguish iron metal from oxides. Figure S1 in the Supporting Information shows the atomic concentration ratios of O and Fe obtained by low-*Z* particle EPMA for ~160 particles of each standard powder and airborne subway sample. The O/Fe values for standard iron metal, magnetite, hematite, and maghemite were 0.08(±0.03), 1.29(±0.10), 1.52(±0.10), and 1.54(±0.11), respectively, of which their corresponding stoichiometry was 0.00, 1.33, 1.50, and 1.50. Iron metal can be clearly differentiated from iron oxides when their morphology and O/Fe data are used together. On the other hand, although the O and Fe atomic ratios obtained for standard particles match well with their stoichiometry, the speciation of subway iron oxides based on the ratio values is not feasible mainly because a wide range of O/Fe ratios were obtained for particles in samples S1 and S2 as shown in Figure S1E, F in the Supporting Information, indicating that most of airborne subway particles are mostly mixtures of iron metal and oxides with fully oxidized or pure metallic particles being rather scare.

The same individual subway particles examined by low-*Z* particle EPMA were investigated further to obtain additional information on the iron oxide species using RMS. Although RMS cannot detect iron metal, the speciation of iron oxides using RMS is quite powerful. Figure S2 in the Supporting Information shows typical Raman spectra obtained from individual standard particles of hematite, magnetite, and maghemite. Strong, characteristic Raman peaks of hematite were observed at 226 and 497 cm^{-1} (two A_{1g} modes) and at 245, 292, 299, 410, and 611 cm^{-1} (five E_g modes), as reported previously.[37] For magnetite, the reported peak positions differed among studies.[37−39] In the present study, as shown in Figure S1(B) in the Supporting Information, three broad, characteristic Raman peaks of magnetite were observed at 298, 530, and 660 cm^{-1}, which are similar to those reported at 302

dx.doi.org/10.1021/ac402406n | Anal. Chem. 2013, 85, 10424−10431

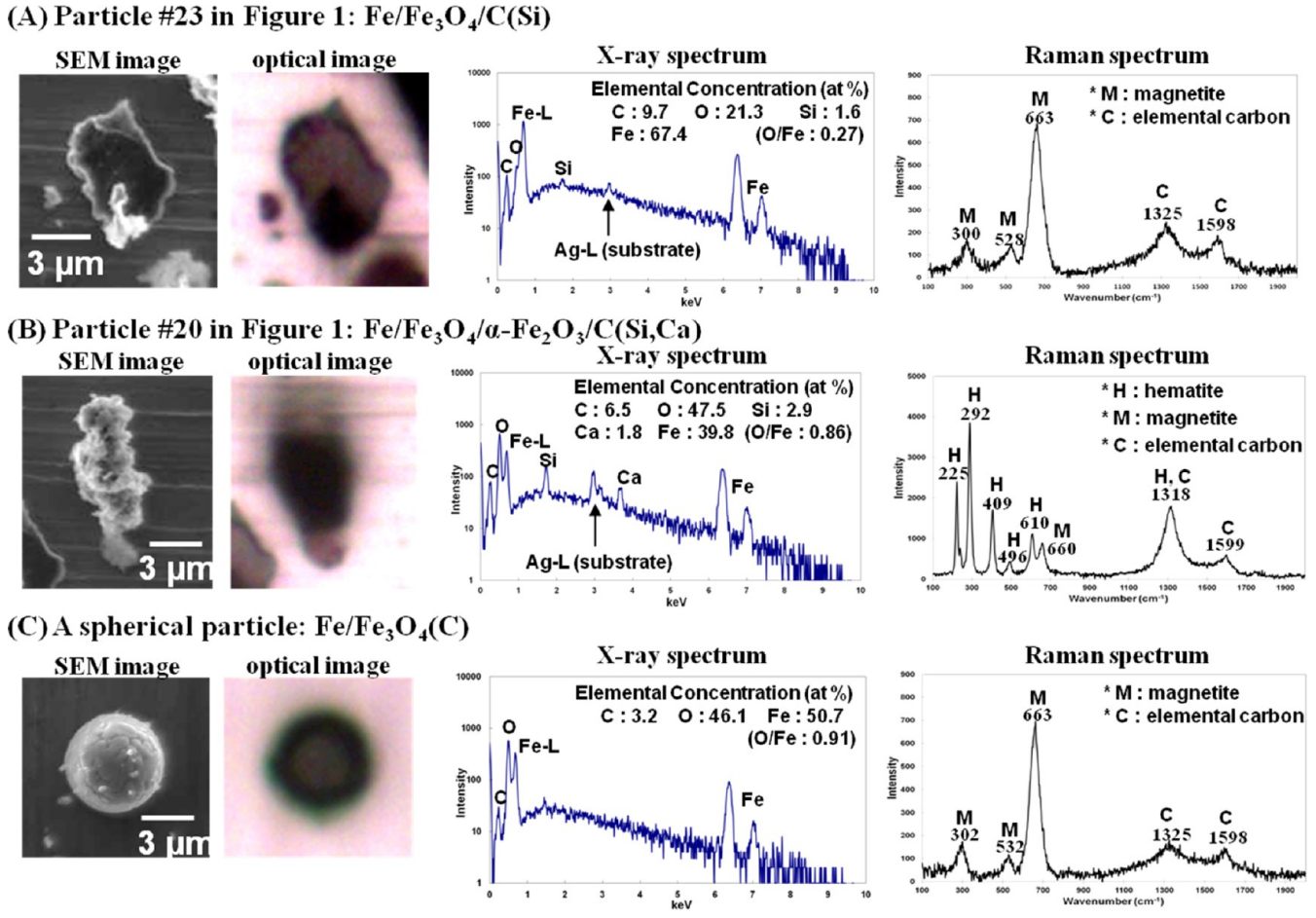

Figure 2. Three exemplar subway particles with their SEIs, optical images, X-ray spectra, and Raman spectra.

and 534 (two T_{2g} mode) and 663 cm^{-1} (one A_{1g} mode).[37] The Raman spectrum of maghemite revealed four broad peaks at ~360 cm^{-1} (one E_g mode), ~500 cm^{-1} (one T_{2g} mode), and ~650 and ~710 cm^{-1} (two A_{1g} modes).[39]

It was reported that magnetite and maghemite can transform thermally into hematite under laser irradiation.[37,38,40] Therefore, it is necessary to determine the analytical conditions to avoid these transformations during the Raman measurements. Indeed, Raman peaks of hematite were observed for standard individual magnetite and maghemite particles by intense-power laser beams, with the intensities of the hematite peaks tending to increase with increasing laser power. Hematite formation induced by the laser beam could be recognized clearly by the different peak intensity, band broadening, band shift, and peak splitting of the beam-induced hematite in its Raman spectra compared to genuine hematite. First, the intensities of the major Raman peaks of genuine hematite were at least 3 times higher than those for the beam-induced one. Second, the shape of the Raman peaks of genuine hematite was much sharper than that of the beam-induced one. In addition, a significant band shift and peak splitting were observed for the beam-induced hematite. These differences observed for genuine and beam-induced hematite suggest that the beam-induced hematite is an amorphous phase whereas genuine hematite is crystalline because crystalline and amorphous hematite structures were reported to provide this type of different behavior.[38,41−43] As a very low laser power is not useful for generating quality Raman signals, the use of 0.7 mW laser power was chosen to examine airborne subway particles without the beam-induced hematite formation as a compromise.

Figure 2A shows an SEI, visible optical image, X-ray spectrum, and Raman spectrum obtained for a typical iron metal particle mixed with magnetite and elemental carbon (assigned as $Fe/Fe_3O_4/C(Si)$). The SEI showed that this angular and sliced particle was rather large (~5.5 μm in its equivalent diameter, which is defined as the diameter of a circular particle with the same area as the particle), and some small particles had aggregated. Its sliced morphology with dark contrast indicated that its major chemical species was iron metal. Indeed, the atomic concentration of Fe element obtained from low-Z particle EPMA was 67.4% compared to an oxygen content of 21.3% (i.e., O/Fe = 0.27). The optical image obtained by the optical microscope in the Raman microspectrometer ensured that the same particle was analyzed by both low-Z particle EPMA and RMS. The Raman spectrum clearly indicates that iron oxide species mixed with iron metal is magnetite with characteristic Raman peaks at 663, 528, and 300 cm^{-1}, as shown in Figure 2A. The carbonaceous species of 9.7 at % from X-ray analysis is elemental carbon or soot based on its characteristic Raman peaks at 1325 and 1598 cm^{-1}.[44−46] As discussed later, XRD results showed a small amount of SiO_2 both in samples S1 and S2, although no Raman peak of SiO_2 was observed due to its low concentration. By considering that major chemical species of the particle are iron metal and magnetite mixed with minor elemental carbon and SiO_2, the relative concentrations of iron metal and magnetite were

dx.doi.org/10.1021/ac402406n | Anal. Chem. 2013, 85, 10424−10431

calculated from the atomic concentration data by X-ray analysis to be ~54% and ~32%, respectively, in the atomic fraction and ~71% and ~24%, respectively, in the weight fraction. Although the morphology of particle no. 23 in Figure 1A was mainly that of metal iron, a significant amount of magnetite most probably formed on the surface based on the atomic concentration data analysis. When the particle was scraped off by wear or friction, its surface would be so active that oxidation of the surface by ambient oxygen would result in magnetite formation.

Figure 2B shows an SEI, visible optical image, X-ray spectrum, and Raman spectrum obtained for a typical particle mixed with magnetite, hematite, and iron metal (assigned as $Fe/Fe_3O_4/\alpha$-Fe_2O_3/C(Si,Ca)). The SEI showed that this angular particle is ~6.4 μm in its equivalent diameter, and the optical image also confirms that X-ray and Raman data could be obtained for this same particle. The Raman spectrum showed that this particle was composed of magnetite and hematite with Raman peaks at 662 cm^{-1} and at the other wavenumbers, respectively.[47] Estimating the contents of magnetite, hematite, and iron metal in this particle is somewhat difficult. However, to perform a rough estimation, the contents of magnetite and hematite in the particle were assumed to be similar as the Raman peak intensities of magnetite and hematite are similar to those obtained for standard magnetite and hematite particles. Accordingly, from the atomic concentration X-ray data of Fe and O (39.8% and 47.5%, respectively, with O/Fe = 0.86), the contents of magnetite, hematite, and iron metal species were calculated approximately as 36%, 26%, and 14%, respectively, in atomic fraction, and 37%, 26%, and 24%, respectively, in weight fraction. The presence of a significant amount of iron metal in this single particle clearly suggests that magnetite and hematite were formed by the surface oxidation of iron metal.

Spherical iron-containing particles were often observed in airborne subway particle samples. Figure 2C shows an SEI, visible optical image, X-ray spectrum, and Raman spectrum obtained for a typical spherical particle of ~5.5 μm diameter. The spherical particles could not be formed through wear and friction processes because such physical abrasion would produce rather angular or sliced particles. In other words, spherical particles can be formed from gaseous or liquid species only under high temperature conditions, which can be achieved in the electric sparks occurring between the catenaries providing electricity to subway trains and pantographs attached to trains. When an electric spark occurred, iron metal in the catenaries and pantograph melts or is vaporized in the air. Either the gaseous iron condensed on a nucleus or a liquid iron metal became a spherical solid as the surrounding temperature decreased. As those spherical particles were mostly micrometers in size, liquid iron metals were probably the precursor of the spherical particles. With further decreases in the surrounding temperature, the surface of the spherical iron particle became oxidized to form magnetite, as observed in the Raman spectrum. From the atomic content of Fe and O of 50.7% and 46.1%, respectively, with O/Fe = 0.91, the contents of magnetite and iron metal species were calculated to be 74% and 25%, respectively, in weight fraction, showing that even the spherical particle that formed from iron either in the gas or liquid phase was not fully oxidized. Most of the spherical particles were magnetite and some were mixed with hematite.

The above three exemplar particles were presented because they were typical particles encountered in samples S1 and S2. The particle types were determined using both low-Z particle EPMA and RMS data as done for the three typical particles. Table 1 lists the relative abundance of the particle types

Table 1. Overall Relative Abundances of the Significantly Encountered Particle Types for Airborne Subway Particles Collected in Daechung (Sample S1) and Yangjae (Sample S2) Stations

	iron species	sample S1 (%)	sample S2 (%)
1	Fe/Fe_3O_4	0.0	0.6
2	Fe/Fe_3O_4/C	6.5	10.8
3	Fe/Fe_3O_4/Si	0.6	0.6
4	Fe/Fe_3O_4/C/Ca	0.0	1.8
5	Fe/Fe_3O_4/C/Si	1.3	3.6
6	Fe/Fe_3O_4/C/Si/Ca	0.6	1.2
7	$Fe/Fe_3O_4/\alpha$-Fe_2O_3	23.4	18.0
8	$Fe/Fe_3O_4/\alpha$-Fe_2O_3/C	20.7	15.7
9	$Fe/Fe_3O_4/\alpha$-Fe_2O_3/C/Si	7.7	6.0
10	$Fe/Fe_3O_4/\alpha$-Fe_2O_3/C/Si/Ca	1.9	2.4
11	Fe_3O_4	1.9	0.0
12	Fe_3O_4/C	3.2	6.6
13	Fe_3O_4/α-Fe_2O_3	10.4	7.4
14	Fe_3O_4/α-Fe_2O_3/C	17.5	20.9
15	Fe_3O_4/α-Fe_2O_3/C/Si	3.2	2.4
16	aluminosilicates/C	0.6	1.2
17	SiO_2/C	0.6	0.6
	total	100.0	100.0

encountered as the number of particles encountered by the total number of particles analyzed. The most common particle type was the one mixed internally with iron metal, magnetite, and hematite (given as $Fe/Fe_3O_4/\alpha$-Fe_2O_3 in Table 1), followed by the ones mixed with magnetite, hematite, and carbon (Fe_3O_4/α-Fe_2O_3/C), with iron metal, magnetite, hematite, and carbon ($Fe/Fe_3O_4/\alpha$-Fe_2O_3/C), with magnetite and hematite (Fe_3O_4/α-Fe_2O_3), with iron metal, magnetite, and carbon (Fe/Fe_3O_4/C), etc. Magnetite was encountered most frequently in samples S1 and S2 (with relative encountering frequencies of ~99% and ~98%, respectively), as internal mixtures with iron metal, hematite, or other elements. The relative abundances of hematite encountered in samples S1 and S2 were ~85% and ~73%, respectively, whereas those of iron metal were ~63% and ~61%, respectively. Among the iron oxides, magnetite is more common than hematite, and hematite is always mixed with iron metal and/or magnetite.

Fine particles can adversely influence human health as smaller particles are more respirable and can penetrate deeper into the lung.[48,49] Such small, submicrometer particles were frequently encountered in samples S1 and S2 as seen in Figure 1A,C (marked as "+" in Figure 1B,D). The number of the marked particles was 75, with their size being 0.59 (±0.16) μm. The relative abundances of chemical species of these particles, obtained by the combined use of low-Z particle EPMA and RMS, are given in Table S2 in the Supporting Information. The results were similar to ones for supermicrometer particles, i.e., the magnetite was almost ubiquitous and the hematite was present as internal mixtures with magnetite and/or iron metal, except the lower relative abundances of iron metal (~42% and ~33% in samples S1 and S2, respectively). This indicates that the smaller particles had higher probability for complete formation of magnetite and/or hematite due to their larger surface-to-volume ratio. As one of major components in the more respirable, submicrometer particles is magnetite, which

dx.doi.org/10.1021/ac402406n | Anal. Chem. 2013, 85, 10424−10431

was reported to be toxic,[12] further work on submicrometer subway particles is needed in terms of public health concern.

This is the first study that clearly elucidated the iron species of airborne underground subway particles generated in tunnels by the combined use of low-Z particle EPMA and RMS techniques. As the outdoor influence was minimal, the chemical nature of the subway particles could be determined with minimal outdoor influence. On the basis of the observation made here, it is clear that iron-containing subway particles were emitted originally as iron metal, either as solid particles (scraped or ground), gaseous or liquid moiety, through wear, friction, or electric spark processes at the rail-wheel-brake or catenaries-pantographs interfaces. When iron metal particles are emitted into the air, their surface and temperature would be active and high, respectively, enough for the particles to be oxidized easily mostly to magnetite by the contact of surrounding air in a relatively short period as the temperature surrounding the particles would quickly decrease to room temperature. According to the iron phase diagram, when oxygen (i.e., 23.1 wt % in the air) is fully available for the oxidation, the most stable iron species is a mixture of α-Fe (iron metal) and Fe_3O_4 at 200−575 °C.[50−53] On the other hand, among the different iron oxides, hematite is the most stable thermodynamically and often the final structure of the transformations of other iron oxides from oxidation process.[51] Magnetite can be oxidized easily to hematite when the temperature is more than 300 °C or the particle size is larger than 300 nm.[51,54] However, the observation of the almost exclusive presence of magnetite in iron-containing subway particles with some hematite species in the mixture strongly suggests that the oxidation product was magnetite. A small portion of magnetite was probably oxidized to hematite due to a kind of air quenching situation that the particles had experienced. Spherical magnetite particles were formed either by the condensation of gaseous iron or by the solidification of liquid iron. The mechanism for the generation of spherical particles might be similar to that of arc welding particles, where magnetite was also reported to form as primary particle species.[55]

Bulk Analysis of Airborne Subway Particles Using XRD. Figure S3 in the Supporting Information shows XRD patterns of samples S1 and S2, where the two patterns are similar except for the presence of $CaCO_3$ (its strongest peak is observed at 29.41° 2θ) in sample S2, indicating that Fe-containing particles in tunnels are generated in a similar manner, i.e., through wear and friction processes at wheel-rail-brake and catenaries-pantographs interfaces. For both samples, the most intense XRD peaks are for Fe_3O_4 (the strongest peak for magnetite is observed at 35.42° 2θ), followed by the peaks for α-Fe_2O_3 (hematite; its strongest peak is at 33.15° 2θ) and iron metal (α-Fe; its strongest peak is at 44.67° 2θ), and SiO_2 (its strongest peak is at 26.64° 2θ). The distinction between magnetite and maghemite was not easy when XRD peaks were broad as the strongest peaks of magnetite and maghemite are in close proximity (the difference in 2θ values for the strongest peaks of two compounds is 0.2−0.5° 2θ). Therefore, it is unclear whether small amounts of maghemite exist in the samples based on the XRD results. On the other hand, as discussed above, the absence of maghemite was confirmed by RMS because the RMS technique could distinguish between magnetite and maghemite.

The intensities of the strongest XRD peaks of the standard SiO_2, $CaCO_3$, iron metal, hematite, and magnetite powders, which were obtained under the same analytical conditions, were ~5600, ~2930, ~510, ~570, and ~590 cps, respectively. On the basis of their XRD sensitivities, the contents of SiO_2, iron metal, hematite, and magnetite for sample S1 were calculated to the first approximation to be 3%, 24%, 30%, and 43%, respectively. The contents of SiO_2, $CaCO_3$, iron metal, hematite, and magnetite for sample S2 were 3%, 5%, 25%, 27%, and 40%, respectively. Magnetite is most abundant in samples S1 and S2, followed by hematite. The sums of the magnetite and hematite contents for samples S1 and S2 were 73% and 67%, respectively. When the contents of iron metal were added to the sums, the contents of iron species in samples S1 and S2 reached to 97% and 92%, respectively. On the other hand, as the detection limits of XRD are normally below 5 wt %, there must be some undetected minor species in the samples. In addition, XRD only detects crystalline species, so that this rough estimation about the relative abundances of iron species is considered qualitative.

In a previous study,[25] most of the floor dust particles collected in an underground subway station were magnetic so that all the floor dusts of the <25 μm size fraction were attracted to a permanent magnet. In this study, all the particles of samples S1 and S2 were attracted to a permanent magnet of 2000 Oe. On the basis of XRD analysis, the nonmagnetic hematite constitutes significant portions of samples S1 and S2 (30% and 27%, respectively). Nevertheless, the observation of all the particles being attracted to the magnet indicates that hematite species in particles of samples S1 and S2 exist mostly as an internal mixture with other magnetic components, as clearly shown by the combined use of low-Z particle EPMA and RMS on a single particle basis.

■ CONCLUSIONS

Iron species in subway particles is of prime interest because of their different toxicity and magnetic properties according to the iron species. In this study, underground subway particle samples were collected in tunnels where the outdoor influence was minimal. This provided clear information on iron-containing particles generated in an underground subway system. For the speciation of iron-containing particles, a newly developed, single particle analytical methodology, which combines low-Z particle EPMA and RMS, was applied to the analysis of the same individual subway particles. The results revealed magnetite, hematite, and iron metal as the major iron species. XRD also confirmed that the major iron-species in the airborne subway particles collected in tunnels are magnetite, hematite, and iron metal.

■ ASSOCIATED CONTENT

Supporting Information

Additional information as noted in text. This material is available free of charge via the Internet at http://pubs.acs.org.

■ AUTHOR INFORMATION

Corresponding Author

*Phone: +82 32 876 7106. Fax: +82 32 874 9207. E-mail: curo@inha.ac.kr.

Present Address

⊥(Y.-S.S.) Exposure, Epidemiology, and Risk Program, Department of Environmental Health, Harvard School of Public Health, Boston, Massachusetts 02215, USA.

Author Contributions

H.-J.E. and H.-J.J. contributed equally to this work.

Notes

The authors declare no competing financial interest.

■ ACKNOWLEDGMENTS

This study was supported by Basic Science Research Programs through the National Research Foundation of Korea (NRF) funded by the Ministry of Education, Science, and Technology (Grants NRF-2011-0008172 and NRF-2012R1A2A1A05026329) and by a French-Korean joint research project funded by the NRF and CNRS (Programme Hubert Curien STAR No. 19040UJ and Grant NRF-2013K1A3A1A21000340).

■ REFERENCES

(1) Furuya, K.; Kudo, Y.; Okinaga, K.; Yamuki, M.; Takahashi, S.; Araki, Y.; Hisamatsu, Y. *J. Trace Microprobe Tech.* **2001**, *19*, 469−485.
(2) Awad, A. H. A. *J. Occup. Health* **2002**, *44*, 112−118.
(3) Johansson, C.; Johansson, P.-A. *Atmos. Environ.* **2003**, *37*, 3−9.
(4) Aarnio, P.; Yli-Tuomi, T.; Kousa, A.; Makela, T.; Hirsikko, A.; Hameri, K.; Raisanen, M.; Hillamo, R.; Koskentalo, T.; Jantunen, M. *Atmos. Environ.* **2005**, *39*, 5059−5066.
(5) Seaton, A.; Cherrie, J.; Dennekamp, M.; Donaldson, K.; Hurley, J. F.; Tran, C. L. *Occup. Environ. Med.* **2005**, *62*, 355−362.
(6) Branis, M. *Atmos. Environ.* **2006**, *40*, 348−356.
(7) Kim, K.; Kim, Y.; Roh, Y. *J. Hazard. Mater.* **2008**, *154*, 440−443.
(8) Park, D.-U.; Ha, K.-C. *Environ. Int.* **2008**, *34*, 629−634.
(9) Murruni, L. G.; Solanes, V.; Debray, M.; Kreiner, A. J.; Davidson, J.; Davidson, M.; Vázquez, M.; Ozafrán, M. *Atmos. Environ.* **2009**, *43*, 4577−4583.
(10) Raut, J.-C.; Chazette, P.; Fortain, A. *Atmos. Environ.* **2009**, *43*, 860−868.
(11) Chillrud, S. N.; Epstein, D.; Ross, J. M.; Sax, S. N.; Pederson, D.; Spengler, J. D.; Kinney, P. L. *Environ. Sci. Technol.* **2004**, *38*, 732−737.
(12) Karlsson, H. L.; Nilsson, L.; Möller, L. *Chem. Res. Toxicol.* **2005**, *18*, 19−23.
(13) Karlsson, H. L.; Ljungman, A. G.; Lindbom, J.; Moller, L. *Toxicol. Lett.* **2006**, *165*, 203−211.
(14) Bachoual, R.; Boczkowski, J.; Goven, D.; Amara, N.; Tabet, L.; On, D.; Leçon-Malas, V.; Aubier, M.; Lanone, S. *Chem. Res. Toxicol.* **2007**, *20*, 1426−1433.
(15) Bigert, C.; Alderling, M.; Svartengren, M.; Plato, N.; De Faire, U.; Gustavsson, P. *Occup. Environ. Med.* **2008**, *65*, 655−658.
(16) Gustavsson, P.; Bigert, C.; Pollan, M. *Am. J. Ind. Med.* **2008**, *51*, 545−547.
(17) Karlsson, H. L.; Holgersson, A.; Möller, L. *Chem. Res. Toxicol.* **2008**, *21*, 726−731.
(18) Salma, I.; Pósfai, M.; Kovács, K.; Kuzmann, E.; Homonnay, Z.; Posta, J. *Atmos. Environ.* **2009**, *43*, 3460−3466.
(19) Loxham, M.; Cooper, M. J.; Gerlofs-Nijland, M. E.; Cassee, F. R.; Davies, D. E.; Palmer, M. R.; Teagle, D. A. H. *Environ. Sci. Technol.* **2013**, *47*, 3614−3622.
(20) Sitzmann, B.; Kendal, M.; Williams, I. *Sci. Total Environ.* **1999**, *241*, 63−73.
(21) Kang, S.; Hwang, H.; Park, Y.; Kim, H.; Ro, C.-U. *Environ. Sci. Technol.* **2008**, *42*, 9051−9057.
(22) Nieuwenhuijsen, M. J.; Gómez-Perales, J. E.; Colvile, R. N. *Atmos. Environ.* **2007**, *41*, 7995−8006.
(23) Querol, X.; Moreno, T.; Karanasiou, A.; Reche, C.; Alastuey, A.; Viana, M.; Font, O.; Gil, J.; De Miguel, E.; Capdevila, M. *Atmos. Chem. Phys.* **2012**, *12*, 5055−5076.
(24) Zhang, W.; Jiang, H.; Dong, C.; Yan, Q.; Yu, L.; Yu, Y. *Geochem. Geophys. Geosyst.* **2011**, *12*, Q06Z25 DOI: 10.1029/2011GC003524.
(25) Jung, H.-J.; Kim, B.; Malek, M.; Koo, Y.; Jung, J.; Son, Y.-S.; Kim, J.-C.; Kim, H.; Ro, C.-U. *J. Hazard. Mater.* **2012**, *213*−*214*, 331−340.
(26) Jung, H.-J.; Kim, B.; Ryu, J.; Maskey, S.; Kim, J.-C.; Sohn, J.; Ro, C.-U. *Atmos. Environ.* **2010**, *44*, 2287−2293.
(27) Kim, B.; Jung, H.-J.; Song, Y.-C.; Lee, M.-J.; Kim, H.; Kim, J.-C.; Sohn, J.; Ro, C.-U. *Asian J. Atomos. Environ.* **2010**, *4*, 97−105.
(28) Sobanska, S.; Hwang, H.; Choël, M.; Jung, H.-J.; Eom, H.-J.; Kim, H.; Barbillat, J.; Ro, C.-U. *Anal. Chem.* **2012**, *84*, 3145−3154.
(29) Ro, C.-U.; Osan, J.; Van Grieken, R. *Anal. Chem.* **1999**, *71*, 1521−1528.
(30) Vekemans, B.; Janssens, K.; Vincze, L.; Adams, F.; Van Espen, P. *X-Ray Spectrom.* **1994**, *23*, 278−285.
(31) Ro, C.-U.; Osan, J.; Szaloki, I.; Van Grieken, R. *Environ. Sci. Technol.* **2000**, *34*, 3023−3030.
(32) Ro, C.-U.; Oh, K.-Y.; Kim, H.; Chun, Y.; Osan, J.; De Hoog, J.; Van Grieken, R. *Atmos. Environ.* **2001**, *35*, 4995−5005.
(33) Ro, C.-U.; Osan, J.; Szaloki, I.; De Hoog, J.; Worobiec, A.; Van Grieken, R. *Anal. Chem.* **2003**, *75*, 851−859.
(34) Ro, C.-U.; Kim, H.; Van Grieken, R. *Anal. Chem.* **2004**, *76*, 1322−1327.
(35) Ryu, J.; Ro, C.-U. *Anal. Chem.* **2009**, *81*, 6695−6707.
(36) Goldstein, J. I.; Newbury, D. E.; Joy, D. C.; Lyman, C.; Echlin, P.; Lifshin, E.; Sawyer, L.; Michael, J. *Scanning Electron Microscopy and X-ray Microanalysis*, 3rd ed.; Springer: New York, 2003.
(37) De Faria, D. L. A.; Venâncio Silva, S.; De Oliveira, M. T. *J. Raman Spectrosc.* **1997**, *28*, 873−878.
(38) Shebanova, O. N.; Lazor, P. *J. Solid State Chem.* **2003**, *174*, 424−430.
(39) Legodi, M. A.; Waal, D. *Dyes Pigments* **2007**, *74*, 161−168.
(40) Guo, C.; Hu, Y.; Qian, H.; Ning, J.; Xu, S. *Mater. Charact.* **2011**, *62*, 148−151.
(41) Gouadec, G.; Colomban, P. *Prog. Cryst. Growth Charact. Mater.* **2007**, *53*, 1−56.
(42) Lutz, H. D.; Haeuseler, H. *J. Mol. Struct.* **1999**, *511*−*512*, 69−75.
(43) Yan, J.; Asami, T.; Kuriyagawa, T. *Precision Eng.* **2008**, *32*, 186−195.
(44) Schmid, J.; Grob, B.; Niessner, R.; Ivleva, N. P. *Anal. Chem.* **2011**, *83*, 1173−1179.
(45) Sadezky, A.; Muckenhuber, H.; Grothe, H.; Niessner, R.; Poschl, U. *Carbon* **2005**, *43*, 1731−1742.
(46) Beyssac, O.; Goffe, B.; Petitet, J.-P.; Froigneux, E.; Moreau, M.; Rouzaud, J.-N. *Spectrochim. Acta* **2003**, *A59*, 2267−2276.
(47) Chourpa, I.; Douziech-Eyrolles, L.; Ngaboni-Okassa, L.; Fouquenet, J.-F.; Cohen-Jonathan, S.; Souce, M.; Marchais, H.; Dubois, P. *Analyst* **2005**, *130*, 1395−1403.
(48) Valavanidis, A.; Fiotakis, K.; Vlachogianni, T. *J. Environ. Sci. Health, Part C* **2008**, *26*, 339−362.
(49) Brauer, M.; Avila-Casado, C.; Fortoul, T. I.; Vedal, S.; Stevens, B.; Churg, A. *Environ. Health Perspect.* **2001**, *109*, 1039−1043.
(50) Greenwood, N. N.; Earnshaw, A. *Chemistry of the Elements*, 2nd ed.; Butterworth-Heinemann: Oxford, U.K., 1997.
(51) Cornell, R. M.; Schwertmann, U. *The Iron Oxides: Structure, Properties, Reactions, Occurrence, And Uses*; VCH: Weinheim, Germany, 1996.
(52) Slattery, J. C.; Peng, K.-Y.; Gadalla, A. M.; Gadalla, N. *Ind. Eng., Chem. Res.* **1995**, *34*, 3405−3410.
(53) Kubaschewski, O. *Iron-Binary Phase Diagrams*; Springer-Verlag: Berlin, 1982.
(54) Colombo, U.; Fagherazzi, G.; Gazzarrini, F.; Lanzavecchia, G.; Sironi, G. *Nature* **1968**, *219*, 1036−1037.
(55) Zimmer, A. T.; Biswas, P. *J. Aerosol Sci.* **2001**, *32*, 993−1008.